Michigan Tech Publications, Part 2

8-21-2021

Earth Imaging From the Surface of the Moon With a DSCOVR/EPIC-Type Camera

Nick Gorkavyi

Simon Carn

Matt DeLand

Yuri Knyazikhin

Nick Krotkov

See next page for additional authors

Authors

Nick Gorkavyi, Simon Carn, Matt DeLand, Yuri Knyazikhin, Nick Krotkov, Alexander Marshak, and et al.

![frontiers in Remote Sensing]

Earth Imaging From the Surface of the Moon With a DSCOVR/EPIC-Type Camera

Nick Gorkavyi[1]*, Simon Carn[2], Matt DeLand[1], Yuri Knyazikhin[3], Nick Krotkov[4], Alexander Marshak[4], Ranga Myneni[3] and Alexander Vasilkov[1]

[1]Science Systems and Applications, Lanham, MD, United States, [2]Department of Geological and Mining Engineering and Sciences, Michigan Technological University, Houghton, MI, United States, [3]Earth and Environment Department, Boston University, Boston, MA, United States, [4]NASA Goddard Space Flight Center, Greenbelt, MD, United States

The Earth Polychromatic Imaging Camera (EPIC) on the Deep Space Climate Observatory (DSCOVR) satellite observes the entire Sun-illuminated Earth from sunrise to sunset from the L1 Sun-Earth Lagrange point. The L1 location, however, confines the observed phase angles to ~2°–12°, a nearly backscattering direction, precluding any information on the bidirectional surface reflectance factor (BRF) or cloud/aerosol phase function. Deploying an analog of EPIC on the Moon's surface would offer a unique opportunity to image the full range of Earth phases, including observing ocean/cloud glint reflection for different phase angles; monitoring of transient volcanic clouds; detection of circum-polar mesospheric and stratospheric clouds; estimating the surface BRF and full phase-angle integrated albedo; and monitoring of vegetation characteristics for different phase angles.

Keywords: DISCOVR EPIC, Moon, phase function, clouds, vegetation

INTRODUCTION

Numerous Low Earth Orbit (LEO) and Geosynchronous Equatorial Orbit (GEO) Earth-observing satellites provide a broad spectral range of viable data; however, it is obtained at the expense of limited geographical (GEO) or temporal (LEO) coverage. Satellites from near-polar Sun-synchronous LEOs have limited observation capabilities at polar latitudes greater than 80° North and South. These polar regions are not observable from geostationary satellites located above the equator. Although current Earth-observing satellites can produce high-resolution views, LEO sensors can only scan a small portion of the surface at a given time, while GEO sensors can provide temporally continuous, though lower-resolution observations of a significant, though incomplete and fixed portion of the Earth's disk. The Earth Polychromatic Imaging Camera (EPIC) on the Deep Space Climate Observatory (DSCOVR) clearly stands apart, observing the entire Sun-illuminated Earth from the L1 Sun-Earth Lagrange point (Marshak et al., 2018). EPIC has an aperture diameter of 30.5 cm, a focal ratio of 9.38, a field of view of 0.61°, and a spatial resolution of ~10 km/pixel. The camera produces 2048 × 2048 pixel images in 10 narrowband channels (317.5, 325, 340, 388, 443, 551, 680, 688, 764, and 779.5 nm). The L1 location, however, restricts phase angles to ~2°–12° (a nearly backscattering direction), depriving the observer of any information on bidirectional surface reflectance factors (BRFs) or on cloud/aerosol phase functions. A compact, lightweight, autonomous EPIC-type camera on the Moon's surface offers a unique opportunity to overcome these limitations and advance Earth science in novel and potentially unanticipated ways (Marshak et al., 2020). An EPIC-Moon camera would work in synergy with the DSCOVR/EPIC instrument, increasing the efficiency of both sensors. Earth science goals of EPIC-Moon are to extend and improve the current
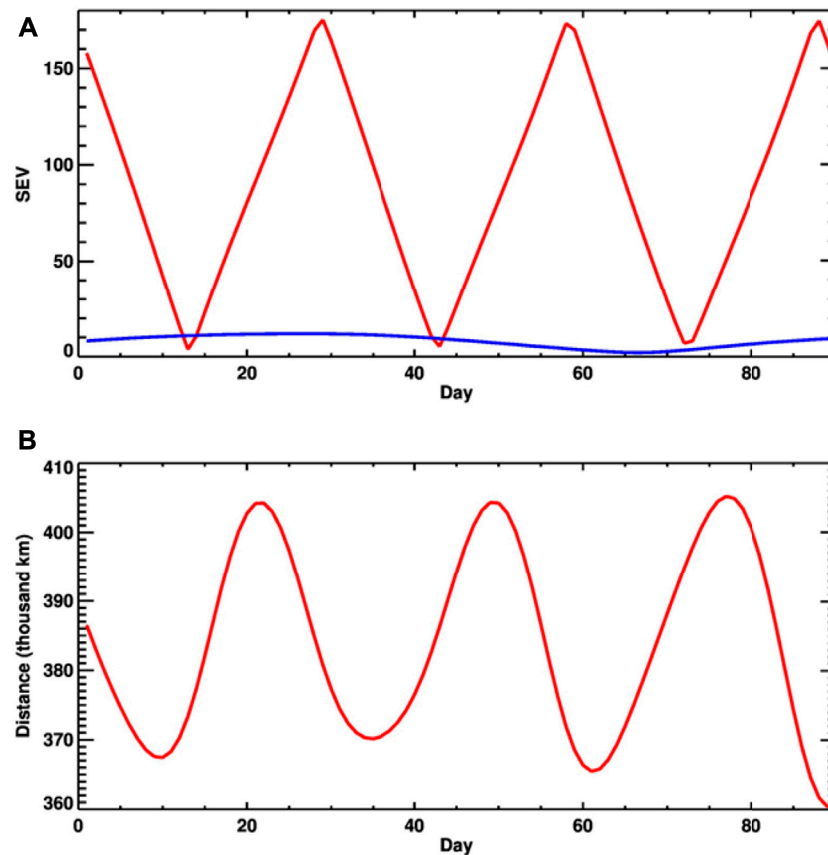
FIGURE 1 | (A) Sun-Earth-Vehicle (SEV) angle for any sunlit Earth object observed from the Moon during the first 3 months of 2021 (red line, data from Espenak, 2021), compared to DSCOVR/EPIC's SEV (blue line, see https://epic.gsfc.nasa.gov/); **(B)** Distance between the Moon and Earth during the same period (Espenak, 2021).

DSCOVR/EPIC Earth imaging by extending spectral coverage, increasing spatial resolution and image cadence, and expanding coverage of circumpolar regions. Assuming the EPIC-Moon camera produces 2048 × 2048 pixel images, the spatial resolution would be ~7 km/pixel for full Earth disk images or ~2 km/pixel for a DSCOVR/EPIC-like field of view of ~0.6°. DSCOVR/EPIC obtains images of the entire sunlit Earth disk every ~60–100 min. Increasing the EPIC-Moon frame rate to obtain images every ~10–15 min will allow much better tracking, for example, of drifting volcanic ash and SO_2 clouds, which can move at speeds of ~100 km/h or more (see *Volcanic SO2 and Ash Clouds*).
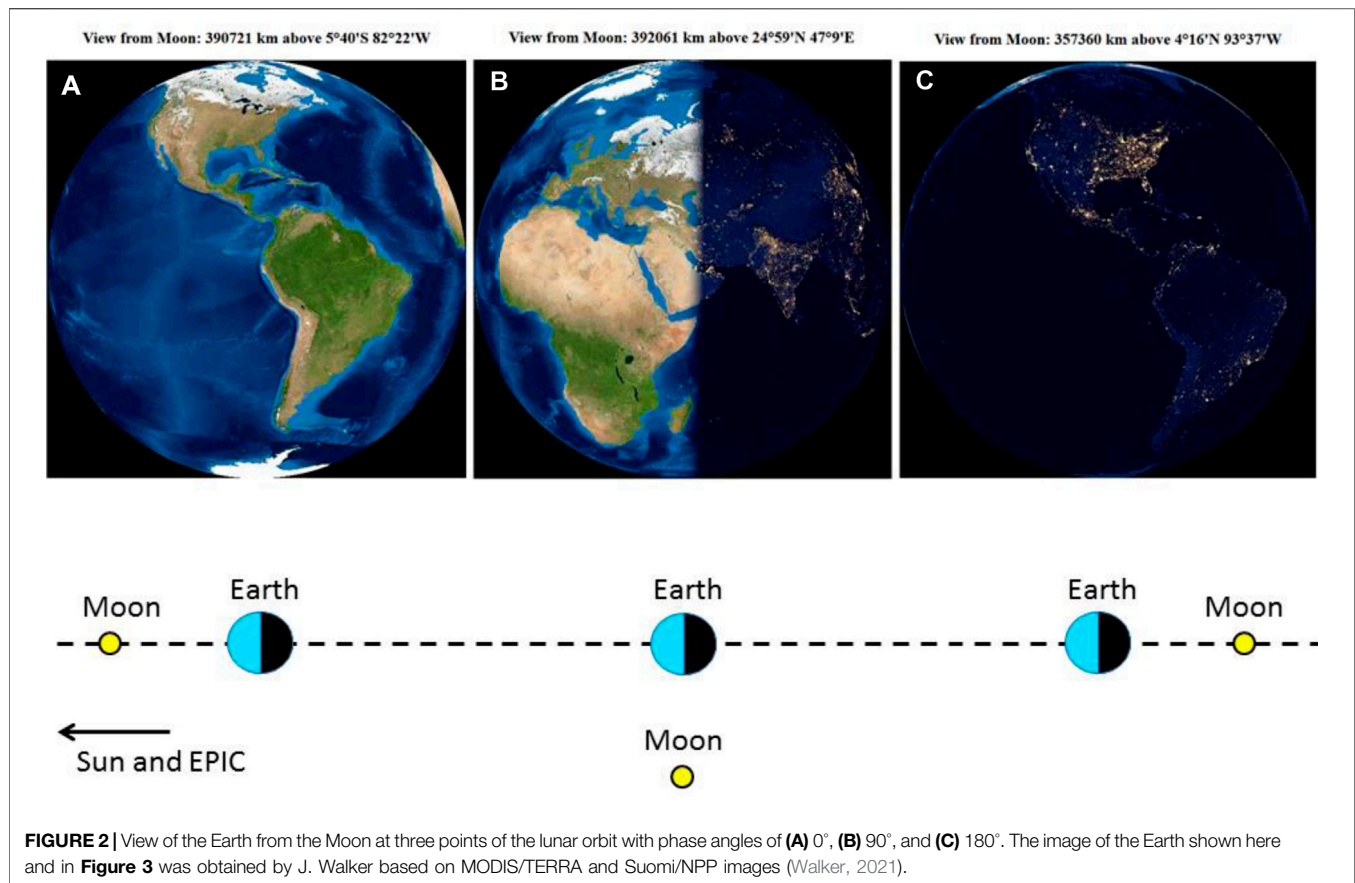
The acquired data will enable retrievals of aerosol scattering phase functions and Earth surface properties. The recent Earth Science Decadal Survey prioritized aerosols, clouds, convection, precipitation, terrestrial vegetation and surface albedo studies in connection with climate change (National Academies of Sciences, 2018). As stated in IPCC AR5 Chapter 7: "Clouds and aerosols continue to contribute the largest uncertainty to estimates and interpretations of the Earth's changing energy budget" (IPCC, 2014). In this paper we analyze the features and potential benefits of an EPIC-like camera located on the Moon (or in lunar orbit).

Note that in the coming years, lunar bases are planned for deployment on the Moon and in lunar orbit, which will be equipped with small telescopes for astronomical observations, for observing the Moon and for laser communication with the Earth. The concept presented here will be useful for assessing the principal possibilities of observing the Earth using telescopes located on the Moon. We do not consider sensors on the Moon as an alternative to sensors located in LEO, GEO, and L1 orbit, but observations from the Moon have a few useful and novel features that are important to discuss and consider in future projects.

PHASE ANGLES OF OBSERVATION FROM L1 AND FROM THE MOON

Here, we compare the phase angles of observation of DSCOVR/EPIC with a sensor placed on the lunar surface. **Figure 1A** shows the Sun-Earth-Vehicle (SEV) angle, which is close to the phase observation angle, for the first 3 months (or 90 days) of 2021.

The SEV angle for DSCOVR/EPIC varies from 11.91° (01/27/2021) to 2.09° (03/07/2021); this allows us to estimate the approximate period of SEV change as ~80 days. During this time, DSCOVR/EPIC's distance from Earth varied from

FIGURE 2 | View of the Earth from the Moon at three points of the lunar orbit with phase angles of **(A)** 0˚, **(B)** 90˚, and **(C)** 180˚. The image of the Earth shown here and in **Figure 3** was obtained by J. Walker based on MODIS/TERRA and Suomi/NPP images (Walker, 2021).

1.54 million km (01/01/2021) to 1.39 million km (02/03/2021). **Figure 1A** shows the SEV angle for the Sun-Earth-Moon (or lunar sensor), which varies from about 0˚ to 180˚ during the lunar month. **Figure 1B** shows the distance between the Moon's and the Earth's centers, which changes in 90 days from 360×10^3 to 405×10^3 km. Therefore, on average, the camera on the Moon is 4 times closer to the Earth than a sensor at the L1 point. The location of Earth and Moon for phase angles of about 0˚, 90˚, and 180˚ is shown in **Figure 2**, along with an assumed view of the Earth from the surface of the Moon. The view of the Earth will be approximately the same from any point in the visible hemisphere of the Moon (from where the Earth is visible). The location of the sensor on the lunar surface is an essential observation factor in terms of solar illumination. A sensor located in the equatorial or mid-latitudes of the Moon will be illuminated by the Sun for only half of the lunar month, remaining in shadow for the second half of the month. This imposes certain constraints on the energy sources for the sensor, as well as on its temperature parameters and calibration.

Scientific equipment could be located at high latitudes on the Moon, for example, in the region of the South Pole, which is an attractive location for a lunar base. There are areas on the rim of Shackleton crater where the Sun illuminates the lunar surface more than 90% of the time. The view of the Earth from the South Pole of the Moon is shown in **Figure 3A**. Note that the Earth is inverted with the North Pole towards the Moon's horizon. The

elevation of the Sun above the Moon's horizon will change. For ~10% of the time, the Sun will be located below the horizon (possible positions of the Sun are shown by dashed circles). Interestingly, lunar eclipses that occur on Earth between 2 and 5 times a year are solar eclipses from the point of view of an observer on the Moon. Unlike an ordinary short-term solar eclipse on Earth, a solar eclipse on the Moon can last up to 108 min. This provides a unique opportunity to make observations without the influence of the atmosphere, for example, to observe phenomena such as the solar corona and its dynamics for an hour and a half, the red ring glow of the Earth's atmosphere, as well as relativistic displacements of the position of stars near the Sun. **Figure 3B** shows the assumed view of a solar eclipse from the South Pole of the Moon.

The proximity to the Earth and wide variations in phase angle accessible by a Moon-based camera offer significant advantages for Earth observation, which we will discuss in the following sections.

SOLAR GLINTS

At least 10% of DSCOVR/EPIC images of Earth contain intensely bright flashes of light over land, not seen by other satellites. The physical origin of these flashes is specular reflection from horizontally floating ice crystals in clouds. The cloud ice
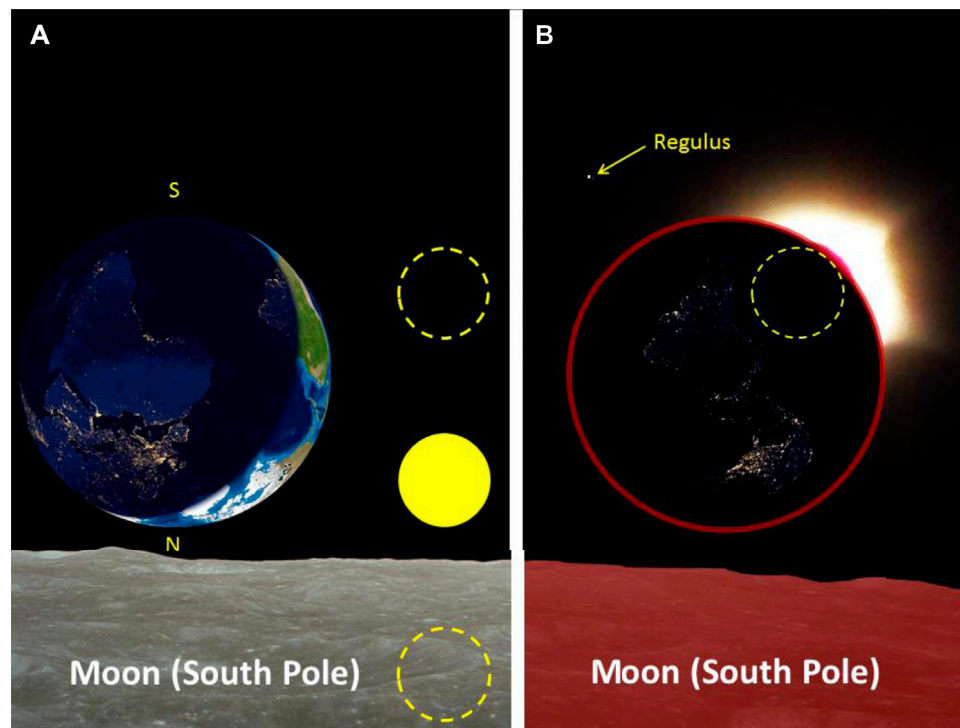
FIGURE 3 | The expected view of the Earth and the Sun from the Moon's South Pole. The picture uses a photo of the lunar surface obtained during the Apollo expedition. Images of the Earth were taken from the Earth and Moon viewer (Walker, 2021). **(A)** The position of the Sun above (or below) the horizon can vary (shown by dashed circles). If the Sun sets behind the disk of the Earth, then a solar eclipse occurs on the Moon–see **(B)**. During a solar eclipse the Earth's atmosphere will glow with red light, and the Sun's corona will glow with white light. Stars will be visible near the Sun's corona. Image **(B)** uses a photograph of the solar corona during an actual solar eclipse on August 21, 2017, where the star Regulus (constellation Leo) is visible (photo by N. Gorkavyi).
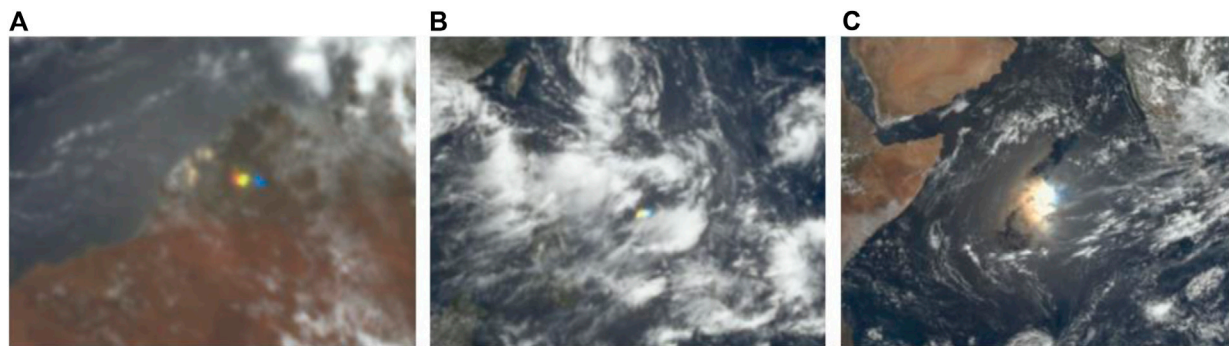

FIGURE 4 | Three examples of glints captured by DSCOVR/EPIC in 2018. The Sun-Earth-Vehicle (SEV) angle is around 9°. Note that the filter wheel used to select EPIC wavelengths causes a time lag between the component images in these red-green-blue (RGB) composites: ~3 min between blue (443 nm) and green (551 nm); ~4 min between blue and red (680 nm). **(A)** Terrestrial glint over Australia from cloud ice crystals on February 13, 2018 (see https://epic.gsfc.nasa.gov/?date=2018-02-13); **(B)** Terrestrial glint over the Pacific Ocean from marine cloud ice crystals on June 15, 2018 (see https://epic.gsfc.nasa.gov/?date=2018-06-15); **(C)** Ocean surface glint on September 17, 2018 (see https://epic.gsfc.nasa.gov/?date=2018-09-17).

crystal glints are also observed over oceans together with glints from the ocean surface. **Figure 4** provides three examples of such flashes.

In order to test the hypothesis that the detected bright flashes over land (see A panel) are caused by specular reflection from horizontally oriented crystals in ice clouds, the measured latitudes

of the detected bright colorful flashes were compared with the theoretical ones that permit specular reflection for a given time of year and color (Marshak et al., 2017). The almost complete coincidence of the measured latitudes for all three colors with the theoretical curve constituted compelling evidence for the specular reflection hypothesis. As a result, it was shown that

tiny hexagonal platelets of ice, floating in the air in nearly perfect horizontal alignment, are likely responsible for the glints observed by EPIC over land. Varnai et al. (2020) also demonstrated EPIC's ability to distinguish ocean surface glints (C panel) from marine ice cloud glints (B panel). Indeed, EPIC's observations in oxygen absorption bands (A-band over ocean) help to uniquely distinguish between ocean surface and high ice clouds. In addition to solar glints from ocean surface and cloud ice, bright reflections of sunlight were also observed from high mountains in the Andes that are likely caused by calm small lakes (Kostinski et al., 2021).

However, the Sun-Earth-satellite geometry of DSCOVR observations is not a particularly favorable one for glint detection. Specular reflection tends to be much stronger for oblique illumination and at grazing angles (Williams and Gaidos, 2008; Robinson et al., 2010). Thus, one expects that in observations at "crescent or half-moon" phases from the Moon, glints will contribute more to the overall planetary radiances-especially when accounting for the decrease in the diffuse radiance when only a portion of the planet's sunlit side is visible. As a function of phase angle, Earth imaging from the Moon will provide ocean/cloud glint reflection for different phase angles than available from GEO, LEO, and L1.

Motivated by EPIC observations of solar glints off the terrestrial atmosphere, it is also important to explore the impact of starlight glints on the detection and characterization of exoplanets. This idea goes back to 1993 when Carl Sagan and colleagues (see p. 715 in Sagan et al., 1993) used the Galileo spacecraft's fly-by observation of Earth as an exoplanet control experiment. Based solely on observations of specular reflection, they deduced that Earth was covered in part by liquid oceans. Their conclusions were based entirely on several Galileo images collected on Dec. 12, 1990 while Galileo was on its way to Jupiter, crossing a line between Sun and Earth. In Sagan et al. (1993) they wrote "*The Galileo mission constitutes an apparently unique control experiment on the ability of fly-by spacecraft to detect life …*." In addition, on p. 718 it was noted that "*… close examination of the images shows a region of specular reflection in ocean but not on land.*" Note that the fraction of oriented ice crystals might be negligible (Breon and Dubrulle, 2004); hence the effect of glints on cloud brightness is small. The sun-glint in EPOXI [two missions: *Deep Impact Extended Investigation* (DIXI) and *Extrasolar Planet Observation and Characterization* (EPOCh)] was relatively minor (though the image was intrinsically blurry; Livengood et al., 2011). However, if some preliminary estimates of the frequency and brightness of solar glints from EPIC are confirmed, specular reflection observations from the Moon's surface could have a longer-term consequence for exoplanet science.

VOLCANIC SO$_2$ AND ASH CLOUDS

Volcanic eruptions periodically emit large quantities of sulfur dioxide (SO$_2$) and aerosol into the free troposphere and stratosphere, with potential impacts on climate, the environment and aviation. After emission, volcanic SO$_2$ converts to liquid sulfate aerosol particles (on timescales of days to months), which can impact climate through the direct aerosol effect on solar radiation. Young volcanic eruption clouds (within a few hours of emission) also contain volcanic ash particles which can be a significant hazard to aviation. Timely monitoring of volcanic SO$_2$ and ash emissions is therefore critical for aviation safety and for assessing the impacts of volcanic eruptions on climate. Volcanic SO$_2$ and ash emissions have been measured using UV satellite instruments on LEO platforms for several decades (Carn et al., 2016), but these observations have low (~daily) temporal resolution. GEO instruments can measure SO$_2$ and volcanic ash in the IR with high cadence, providing critical data for operational detection of volcanic eruptions (e.g., Pavolonis et al., 2018), but are unable to detect volcanic clouds at latitudes above ~70–80° and retrievals become noisy (with lower sensitivity) towards the edge of the GEO field-of-view. LEO satellites provide coverage of the polar regions, but with relatively low cadence and without a synoptic, hemispheric imaging capability.

DSCOVR/EPIC is able to detect volcanic SO$_2$ and ash emissions (Carn et al., 2018) and has now demonstrated the value of observations from L1 for observing high-latitude volcanic eruptions. A major eruption of Raikoke volcano (Kuril Islands, Russia) in June 2019 emitted SO$_2$ and ash clouds that initially drifted north to high latitudes and were measured with hourly cadence by EPIC (**Figure 5**). EPIC was able to map the extensive Raikoke volcanic SO$_2$ clouds in single images with no temporal gaps, in contrast to LEO instruments, elucidating the dynamics of SO$_2$ transport. Such high-latitude eruptions occur quite frequently in active volcanic regions such as Kamchatka, the Kuril Islands, Alaska and the Aleutian Islands, and Iceland. In addition to Raikoke, notable high-latitude volcanic eruptions include Kasatochi (Aleutian Islands, United States) in 2008, Sarychev Peak (Kuril Islands, Russia) in 2009, Holuhraun (Iceland) in 2014–15 and Alaid (Kuril Islands, Russia) in 1981. Each of these eruptions produced extensive SO$_2$ clouds that drifted over the Arctic region. The Southern Hemisphere has fewer active volcanoes at high latitudes, but nevertheless, significant eruptions such as Cerro Hudson (Chile) in 1991 and Cordon Caulle (Chile) in 2011 produced volcanic clouds that drifted south around Antarctica. Hence there is a need for improved observations of volcanic clouds at high latitudes, given the importance of the polar regions in the context of climate change. An EPIC-like instrument on the Moon would provide synoptic imaging of the polar regions with higher spatial resolution and higher cadence than provided by DSCOVR/EPIC at L1.

In addition to improved cadence and spatial resolution of volcanic SO$_2$ and ash measurements, EPIC-Moon observations would offer advantages over DSCOVR/EPIC for volcanic aerosol detection and retrieval. Aerosol particles in volcanic clouds include liquid sulfate aerosol, which are spherical, plus volcanic ash particles (glass shards and crystal fragments) which can have highly irregular shapes. Ash particle phase functions depend on effective particle size but are typically strongly forward scattering at UV wavelengths (Krotkov et al., 1997; Krotkov et al., 1999), which is a limitation for observations
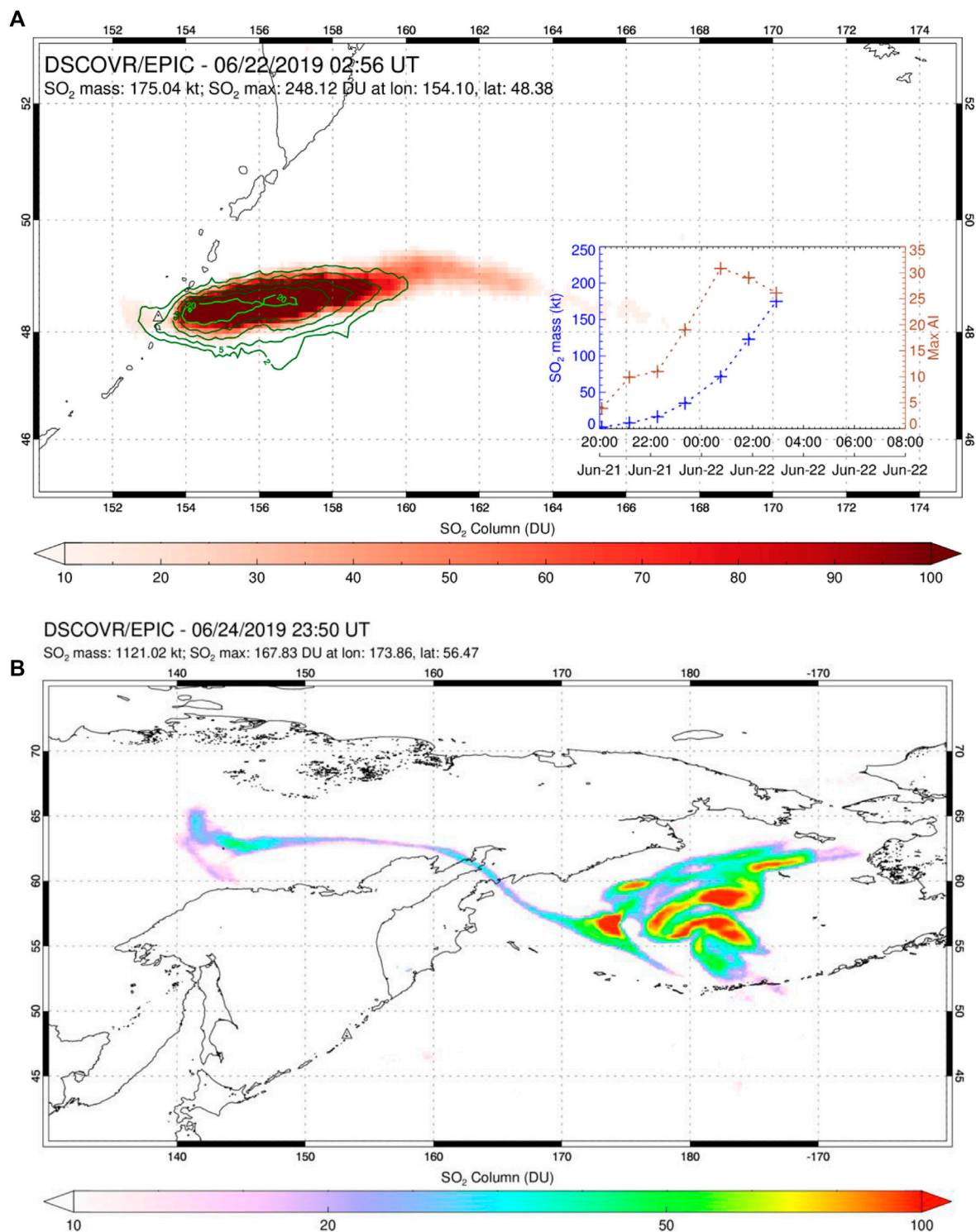
FIGURE 5 | (A) EPIC SO$_2$ and UV Aerosol Index (UVAI; *green contours*) measurements during the eruption of Raikoke volcano (Kuril Islands, Russia; *triangle*) on June 22, 2019 at 02:56 UT. The UVAI is used to detect volcanic ash. Inset lower right shows a time-series of volcanic SO$_2$ mass and UVAI derived from EPIC measurements with hourly cadence during the eruption. **(B)** EPIC SO$_2$ retrieval for the high-latitude Raikoke volcanic cloud on June 24 at 23:50 UTC. EPIC was able to capture this extensive, high-latitude volcanic cloud in single synoptic images with hourly cadence, whereas such latitudes are towards the edge of the geostationary (GEO) field-of-view and can only be covered by multiple overpasses of polar-orbiting (LEO) instruments (with inter-orbit gaps of ~100 min).

of volcanic ash from L1 (in the backscattering direction). Due to changes in the phase function with particle size, the ability to discriminate between ash particle sizes in a volcanic cloud increases if observations at different scattering angles are available.

Studies of particle shape effects on the phase function indicate that, at UV wavelengths, particle non-sphericity leads to increased scattering at side-scattering angles (120–140°) and decreases at backscattering angles (Krotkov et al., 1997; Krotkov et al., 1999). If ash particles are assumed to be spherical, UV retrievals of ash optical depth will be underestimated at backscattering angles (i.e., EPIC observations from L1) and overestimated at side-scattering angles. Scattering angles near 150° are optimal for optical depth retrievals independent of particle shape. Hence the larger range of phase angles accessible from EPIC-Moon observations could potentially improve the accuracy of UV volcanic ash retrievals.

POLAR MESOSPHERIC CLOUDS AND POLAR STRATOSPHERIC CLOUDS

Numerous phenomena in the Earth's middle and upper atmosphere occur in layers that are typically limited in vertical extent but cover extensive horizontal areas. Examples include polar stratospheric clouds (PSCs) and polar mesospheric clouds (PMCs). Localized injections into the stratosphere from below, such as ash plumes from volcanic eruptions or smoke from pyrocumulonimbus (pyroCb) wildfire events, can also be transported by strong winds to spread globally and last for months. Measurements with limb viewing geometry are valuable in studying these phenomena because the long line-of-sight through the atmosphere can enhance an otherwise faint signal. Examples of limb observations for each type of event have been published recently (Tsuda et al., 2018; Bourassa et al., 2019; DeLand et al., 2020; DeLand and Gorkavyi, 2020; Torres et al., 2020; Gorkavyi et al., 2021). The source material for these clouds and plumes are primarily composed of relatively small particles (tens of nm to few hundred nm in radius), with varying composition (PMC = water ice, PSC = nitric acid trihydrate, volcano = ash, and sulfate, pyroCb = smoke). The small size of these particles means that the intensity of observed reflected light (near-UV, visible, near-IR) will be governed by Mie theory, and thus will vary significantly as a function of scattering angle. The periodic variation of observing phase angle shown in **Figure 1A** for a lunar sensor would be quite valuable for these atmospheric measurements. The resulting variation in phase function (and thus observed signal) can be used to help distinguish between different assumptions about particle size distribution and composition, which also affect the phase function.

MONITORING VEGETATION

Natural terrestrial surfaces scatter shortwave radiation into an angular reflectance pattern or Bidirectional Reflectance Factor
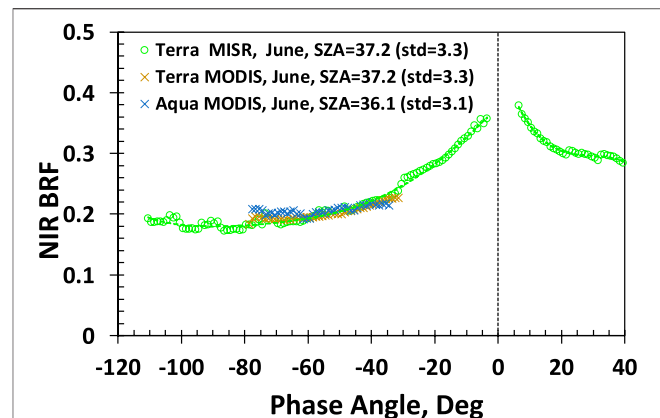

FIGURE 6 | Near-infrared BRF of Amazonian forests confined between 0° to 10°S and 60°W to 70°W from Terra MISR, Terra MODIS, and Aqua MODIS sensors for the period between June 25 and July 10 accumulated over a 7-years period from 2001 to 2008. The MISR sensor views the Earth's surface with nine cameras simultaneously, as opposed to the two MODIS sensors, which are capable of only one view each. The MISR observing geometry allows for measurements of angular signatures over a wider range of phase angles.

(BRF). In vegetation canopies, the finite size of scatterers (e.g., leaves, coniferous shoots, etc.) can cast shadows. This causes the canopy "hot spot" effect, i.e., a sharp increase in canopy reflected radiation as the scattering direction approaches the direction to the Sun (**Figure 6**) (Ross and Marshak, 1988; Knyazikhin and Marshak, 1991; Kuusk, 1991; Myneni et al., 1991; Qin et al., 1996; Gerstl, 1999). The hot spot phenomenon is strongly correlated with canopy architectural parameters such as foliage size and shape, crown geometry and within-crown foliage arrangement, foliage grouping, leaf area index and its sunlit fraction (Ross and Marshak, 1991; Qin et al., 1996; Goel et al., 1997; Knyazikhin et al., 1998; Qin et al., 2002; Schull et al., 2011; Yang et al., 2017; Pisek et al., 2021). Angular signatures that include the hot spot region are critical for monitoring phenological changes in dense vegetation such as equatorial forests (Bi et al., 2015).

Sensors onboard Earth-orbiting satellites sample reflectance over swaths at a specific local solar time, or over a specific area of the sunlit Earth. Such intrinsic sampling limits makes observations of the hot spot rare in occurrence. For example, the cross-track MODIS scanners on the Terra and Aqua near-polar Sun-synchronous orbits can observe about 30–35% of equatorial Amazonian rainforests along the hotspot directions around the Equinoxes. No such observations are available from May to July and November to December (**Figure 7**). The Multiangle Imaging Spectroradiometer (MISR) on the Terra satellite views the Earth's surface with nine cameras simultaneously, as opposed to the two MODIS sensors, which are capable of only one view each. The MISR observing strategy allows for a better angular variation of surface BRFs in the equatorial zone (**Figure 7**). However, spatially and temporally varying phase angles could be far from zero, making global observation of the hot spot phenomenon impossible. A spectroradiometer on the Moon's surface offers a unique opportunity to provide observations of every region of the
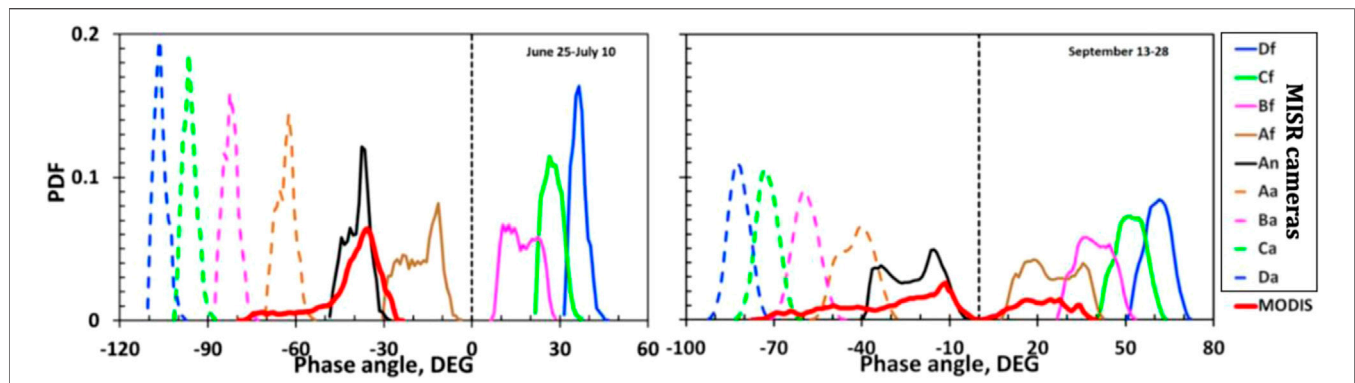
FIGURE 7 | Probability density function (pdf) of the phase angle during 25 June to 10 July and 13–28 September periods over Amazonian rainforests (0°–10°S and 60°W to 70°W) for Terra MODIS and MISR sun-sensor geometries derived from MODIS and MISR data acquired from June 2000 to May 2008. MISR instrument uses nine cameras to view the Earth's surface in the forward and backward directions along the spacecraft's flight track with nominal viewing zenith angles relative to the surface reference ellipsoid of 0.0° (camera An), 26.1° (Af and Aa), 46.5° (Bf and Ba), 60.0° (Cf and Ca), and 70.5° (Df and Da). The 360 km swath width covers the globe in 9 days. MODIS is a single view sensor that scans the Earth's surface across the spacecraft flight track. It has a viewing swath width of 2,330 km and views the entire surface of the Earth every 1–2 days. From Song et al., 2018.

Earth from sunrise to sunset at a full range of phase angles. Here, we discuss an application of surface reflectance data at a full range of phase angles to monitor phenological changes in equatorial forests.

Tropical forests account for approximately one-third of Earth's terrestrial gross primary productivity and one-half of Earth's carbon stored in terrestrial vegetation (Lewis et al., 2009; Pan et al., 2011; Lewis et al., 2015; Hubau et al., 2020). They play an essential role in surface energy partitioning and the Earth's carbon cycle and consequently impact regional climate (Cook et al., 2020; Forzieri et al., 2020). Because of its large geographical extent, any perturbations within this system can have significant impacts on climate and on the carbon and water cycles. Monitoring the spatial patterns, intra-annual seasonality and their controls, inter-annual variability and long-term trends in the structure and functioning of rainforests is crucial to our understanding of how these biodiverse and productive ecosystems will respond to future climate change, disturbances and human appropriation (Cox et al., 2004; Cox et al., 2013; Guimberteau et al., 2017).

Monitoring of dense vegetation such as equatorial rainforests is a challenge for optical remote sensing because reflection of solar radiation saturates and becomes weakly sensitive to vegetation changes. At the same time, satellite data are strongly influenced by changing sun-sensor geometry. This makes it difficult to discriminate between vegetation changes and sun-sensor geometry effects. Commonly used approaches for interpretation of satellite data from single-viewing sensors consider the viewing and solar zenith angle (SZA) dependence of reflected radiation as a source of noise or error, requiring a correction or normalization to a "standard" sun-sensor geometry. **Figure 6** shows the BRF in the NIR spectral band from single-angle Terra and Aqua MODIS sensors acquired over Amazonian rainforests. Their values are almost constant: they vary between 0.18 and 0.23 with mean, standard deviation and coefficient of variation of 0.2, 0.08 and 4%, respectively. Most surface BRF models would interpret such observations as radiation scattered
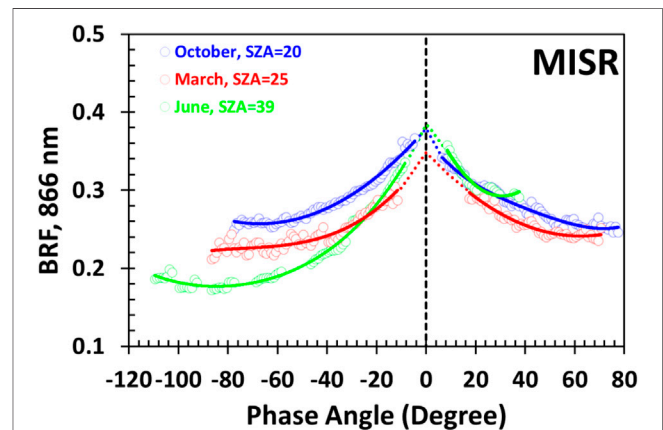

FIGURE 8 | Angular signatures of NIR reflectance of Amazonian forests in March (5 Mar to 20 Mar), June (25 Jun to 10 Jul), and October (15 Oct to 30 Oct) derived from MISR data.

by Lambertian surfaces. Transformation of such data to a fixed, standard sun-sensor geometry therefore invokes statistical assumptions that may not apply to specific scenes. The lack of information on the angular variation of forest-reflected radiation introduces model uncertainties that in turn may have significant impacts on interpretation of satellite data. For example, studies of Amazon forest seasonality based on analyses of data from single-viewing sensors disagree on whether there is more greenness in the dry season than in the wet season: the observed variations in the forest BRF were explained by an increase in the leaf area, an artifact of sun-sensor geometry and changes in leaf age through the leaf flush (Huete et al., 2006; Myneni et al., 2007; Brando et al., 2010; Samanta et al., 2012; Morton et al., 2016; Saleska et al., 2016). Conflicting conclusions among these studies arise from different interpretations of surface reflectance data acquired under saturation conditions (Bi et al., 2015).

Figure 8 shows seasonal changes in NIR BRF of Amazonian forests. The seasonal cycle consists of a short dry season from June to October, and a long wet season thereafter. There are several noteworthy features in the variation of angular signatures. First, a distinct decrease in reflected NIR radiation in all viewing directions from the early (October) to middle (March) part of the wet season with no change in the overall shape of the angular signatures. The SZA is almost the same. The observed downward shift under similar illumination conditions can only result from a change in canopy properties (Bi et al., 2015). Second, the shape of the BRF changes from the beginning (June) to late (October) dry season. Illumination conditions are different in these months. A higher or equal reflectance at lower SZA relative to that at higher SZA always indicates an increase in leaf area and foliage scattering properties (Bi et al., 2015). Moreover, the intersection point of BRFs acquired in these months deviates significantly from that predicted by the reciprocity theorem for identical canopies under different illumination conditions, suggesting that Amazonian forests cannot be similar at the beginning and end of dry seasons (Bi et al., 2015). These examples illustrate that the availability of BRFs over equatorial forests at a full range of the phase angle under different illumination conditions will make monitoring their changes more reliable.

Improved measurements of albedo of the components of Earth's land surface–snow, ice, vegetation, and soil are among the priority targeted observables that were ranked in the Earth Science Decadal Survey as most important or very important (National Academies of Sciences, 2018, p. 229). Spectral albedo (or directional hemispherical reflectance in remote sensing nomenclature) is the integral of the cosine weighted BRF over scattering directions. Measurements of radiation scattered by the land surface in all directions are therefore required to perform the integration. An EPIC-like camera on the Moon's surface can provide frequent observations of every region of the Earth in the full range of scattering directions. The availability of such data will undoubtedly advance our ability to model evapotranspiration, snowmelt, and retrospective reconstruction of the snow water equivalent, which are critical for accurate description of the surface radiation balance (National Academies of Sciences, 2018, p. 227).

LUNAR ENVIRONMENT

Forward scattering conditions create advantages for observing the lunar dust cloud. The lunar dust exosphere is an important factor for the long-term residence of astronauts on the Moon, as well as for the functioning of scientific equipment on the lunar surface and orbiters (Elphic et al., 2014; Richard et al., 2018). Telescopic limb observations of the scattering of sunlight (or starlight) from the lunar dust cloud would help construct a 3D model of the lunar dust exosphere (Richard et al., 2018). We believe that preliminary information regarding the effectiveness of observing the Earth from the lunar surface can be obtained by analyzing photographs of the Earth obtained using the navigation cameras of the lunar rover VIPER (Colaprete et al., 2021). In addition, analysis of photographs from VIPER cameras taken under conditions of

forward scattering of both sunlight and reflected light of the Earth can provide useful information for comparison with models of lunar dust (Richard et al., 2018). A similar program was implemented for the Cosmic Background Explorer (COBE) data and the model of the zodiacal dust cloud (Gorkavyi et al., 2000). Observations from the Moon will help improve existing models of the zodiacal cloud, which is important for astronomical observations, e.g., by the James Webb Space Telescope (JWST) in particular. Even a small meteoroid with a mass of 5 kg can excavate a ~10 m crater, ejecting 75 tons of lunar regolith and rock on ballistic trajectories above the Moon (Dunbar, 2021). However, "*The lunar impact rate is very uncertain because observations for objects in this mass range are embarrassingly few*" (Speyerer et al., 2016). Accurate assessment of the meteorite hazard is required for the effective and safe implementation of the Artemis program (Elphic et al., 2014). Using the Earth's atmosphere as a detector, EPIC-Moon imaging of the night-side and limb of the Earth will detect atmospheric impacts (either by a flash or from dispersion of meteoritic dust clouds; see Gorkavyi et al., 2013) from potentially threatening small (<10 m) asteroids in the vicinity of Earth, thus improving the current highly uncertain estimates.

CONCLUSION

Deploying an analog of DSCOVR/EPIC on the Moon's surface would offer a unique opportunity to image the full range of Earth phases, potentially advancing Earth science in many ways:

1) observing ocean/cloud glint reflection for different phase angles;
2) comprehensive whole-globe monitoring of transient volcanic and aerosol clouds (smoke, dust), including the strategically important (for climate studies) polar regions not covered by GEO missions;
3) detecting of polar mesospheric and stratospheric clouds *via* whole-Earth limb imaging;
4) estimating surface BRF and full phase-angle integrated albedo;
5) monitoring and quantifying changes in vegetated land;
6) simultaneous imaging of the day and night parts (i.e., the twilight zone) during crescent phases of the Earth and shadowed parts illuminated by the Moon.

DATA AVAILABILITY STATEMENT

The original contributions presented in the study are included in the article/supplementary material, further inquiries can be directed to the corresponding author.

AUTHOR CONTRIBUTIONS

NG, SC, MD, YK, AM, and RM developed computer codes and algorithms, analyzed the results and wrote the manuscript. NK,

AM, and AV set the task of developing, supported the development of the algorithm, analyzed the results and wrote the manuscript.

REFERENCES

Bi, J., Knyazikhin, Y., Choi, S., Park, T., Barichivich, J., Ciais, P., et al. (2015). Sunlight mediated seasonality in canopy structure and photosynthetic activity of Amazonian rainforests. *Environ. Res. Lett.* 10, 064014. doi:10.1088/1748-9326/10/6/064014

Bourassa, A. E., Rieger, L. A., Zawada, D. J., Khaykin, S., Thomason, L. W., and Degenstein, D. A. (2019). Satellite limb observations of unprecedented forest fire aerosol in the stratosphere. *J. Geophys. Res. Atmos.* 124, 9510–9519. doi:10.1029/2019JD030607

Brando, P. M., Goetz, S. J., Baccini, A., Nepstad, D. C., Beck, P. S. A., and Christman, M. C. (2010). Seasonal and interannual variability of climate and vegetation indices across the Amazon. *Proc. Natl. Acad. Sci.* 107, 14685–14690. doi:10.1073/pnas.0908741107

Bréon, F.-M., and Dubrulle, B. (2004). Horizontally oriented plates in clouds. *J. Atm. Sci.* 61, 2888–2898. doi:10.1175/JAS-3309.1

Carn, S. A., Clarisse, L., and Prata, A. J. (2016). Multi-decadal satellite measurements of global volcanic degassing. *J. Volcanology Geothermal Res.* 311, 99–134. doi:10.1016/j.jvolgeores.2016.01.002

Carn, S. A., Krotkov, N. A., Fisher, B. L., Li, C., and Prata, A. J. (2018). First Observations of Volcanic Eruption Clouds from the L1 Earth-Sun Lagrange Point by DSCOVR/EPIC. *Geophys. Res. Lett.* 45, 11456–11464. doi:10.1029/2018GL079808

Colaprete, A., Elphic, R. C., Shirley, M., Ennico-Smith, K., Lim, D. S. S., Zacny, K., et al. (2021). The Volatiles Investigating Polar Exploration Rover (VIPER) Mission. 15-19 March, 2021. LPI Contribution No. 2548, id.1523, https://ui.adsabs.harvard.edu/#abs/2021LPI.52.1523C/abstract.52nd Lunar and Planetary Science Conference.

Cook, K. H., Liu, Y., and Vizy, E. K. (2020). Congo Basin drying associated with poleward shifts of the African thermal lows. *Clim. Dyn.* 54, 863–883. doi:10.1007/s00382-019-05033-3

Cox, P. M., Betts, R. A., Collins, M., Harris, P. P., Huntingford, C., and Jones, C. D. (2004). Amazonian forest dieback under climate-carbon cycle projections for the 21st century. *Theor. Appl. Climatol* 78, 137–156. doi:10.1007/s00704-004-0049-4

Cox, P. M., Pearson, D., Booth, B. B., Friedlingstein, P., Huntingford, C., Jones, C. D., et al. (2013). Sensitivity of tropical carbon to climate change constrained by carbon dioxide variability. *Nature* 494, 341–344. doi:10.1038/nature11882

DeLand, M. T., Bhartia, P. K., Kramarova, N., and Chen, Z. (2020). OMPS LP observations of PSC variability during the NH 2019-2020 season. *Geophys. Res. Lett.* 47, e2020GL090216. doi:10.1029/2020gl090216

DeLand, M. T., and Gorkavyi, N. (2021). PMC observations from the OMPS Limb Profiler. *J. Atmos. Solar-Terrestrial Phys.* 213, 105505. doi:10.1016/j.jastp.2020.105505

Dunbar, B. (2021). *About Lunar Impact Monitoring.* Huntsville, AL: NASA. https://www.nasa.gov/centers/marshall/news/lunar/overview.html.

Elphic, R. C., Delory, G. T., Delory, G. T., Hine, B. P., Mahaffy, P. R., Horanyi, M., et al. (2014). The Lunar Atmosphere and Dust Environment Explorer Mission. *Space Sci. Rev.* 185, 3–25. doi:10.1007/s11214-014-0113-z

Espenak, F. (2021). *Geocentric Ephemeris for the Sun, Moon and Planets.* http://astropixels.com/ephemeris/moon/moon2021.html.

Forzieri, G., Miralles, D. G., Ciais, P., Alkama, R., Ryu, Y., Duveiller, G., et al. (2020). Increased control of vegetation on global terrestrial energy fluxes. *Nat. Clim. Chang.* 10, 356–362. doi:10.1038/s41558-020-0717-0

Gerstl, S. A. W. (1999). Building a global hotspot ecology with Triana data. *Remote Sensing Earth Sci. Ocean, Sea Ice Appl.* 3868, 184–194. doi:10.1117/12.373094

Goel, N. S., Qin, W., and Wang, B. (1997). On the estimation of leaf size and crown geometry for tree canopies from hotspot observations. *J. Geophys. Res.* 102, 29543–29554. doi:10.1029/97JD01110

Gorkavyi, N., Krotkov, N., Li, C., Lait, L., Colarco, P., Carn, S., et al. (2021). Tracking aerosols and SO2 clouds from the Raikoke eruption: 3D view from satellite observations. *Atmos. Meas. Tech.*, 58, 2021 . amt-2021. doi:10.5194/amt-2021-58

Gorkavyi, N., Ozernoy, L. M., Mather, J. C., and Taidakova, T. A. (2000). "The NGST and the zodiacal light in the Solar system," in *NGST Science and Technology Exposition.* Editors E. P. Smith and K. S. Long (San Francisco: ASP Series), 207, 462–467.

Gorkavyi, N., Rault, D. F., Newman, P. A., Da Silva, A. M., and Dudorov, A. E. (2013). New stratospheric dust belt due to the Chelyabinsk bolide. *Geophys. Res. Lett.* 40, 4728–4733. doi:10.1002/grl.50788

Guimberteau, M., Ciais, P., Ducharne, A., Boisier, J. P., Dutra Aguiar, A. P., Biemans, H., et al. (2017). Impacts of future deforestation and climate change on the hydrology of the Amazon Basin: a multi-model analysis with a new set of land-cover change scenarios. *Hydrol. Earth Syst. Sci.* 21, 1455–1475. doi:10.5194/hess-21-1455-2017

Hubau, W., Lewis, S. L., Phillips, O. L., Affum-Baffoe, K., Beeckman, H., Cuní-Sanchez, A., et al. (2020). Asynchronous carbon sink saturation in African and Amazonian tropical forests. *Nature* 579, 80–87. doi:10.1038/s41586-020-2035-0

Huete, A. R., Didan, K., Shimabukuro, Y. E., Ratana, P., Saleska, S. R., Hutyra, L. R., et al. (2006). Amazon rainforests green-up with sunlight in dry season. *Geophys. Res. Lett.* 33, L06405. doi:10.1029/2005GL025583

IPCC (2014). *Fifth Assessment Report (AR5).* https://www.ipcc.ch/assessment-report/ar5/.

Knyazikhin, Y., and Marshak, A. (1991). "Fundamental Equations of Radiative Transfer in Leaf Canopies, and Iterative Methods for Their Solution," in *Photon-vegetation interactions: applications in plant physiology and optical remote sensing.* Editors R. B. Myneni and J. Ross (Berlin Heidelberg: Springer-Verlag), 9–43. doi:10.1007/978-3-642-75389-3_2

Knyazikhin, Y., Martonchik, J. V., Myneni, R. B., Diner, D. J., and Running, S. W. (1998). Synergistic algorithm for estimating vegetation canopy leaf area index and fraction of absorbed photosynthetically active radiation from MODIS and MISR data. *J. Geophys. Res.* 103, 32257–32275. doi:10.1029/98JD02462

Kostinski, A., Marshak, A., and Várnai, T. (2021). Deep space observations of terrestrial glitter. *Earth Space Sci.* 8, e2020EA001521. doi:10.1029/2020EA001521

Krotkov, N. A., Flittner, D. E., Krueger, A. J., Kostinski, A., Riley, C., Rose, W., et al. (1999). Effect of particle non-sphericity on satellite monitoring of drifting volcanic ash clouds. *J. Quantitative Spectrosc. Radiative Transfer* 63, 613–630. doi:10.1016/S0022-4073(99)00041-2

Krotkov, N. A., Krueger, A. J., and Bhartia, P. K. (1997). Ultraviolet optical model of volcanic clouds for remote sensing of ash and sulfur dioxide. *J. Geophys. Res.* 102 (D18), 21891–21904. doi:10.1029/97JD01690

Kuusk, A. (1991). "The Hot Spot Effect in Plant Canopy reflectance," in *Photon-vegetation interactions: applications in plant physiology and optical remote sensing.* Editors R. B. Myneni and J. Ross (Berlin Heidelberg: Springer-Verlag), 139–159. doi:10.1007/978-3-642-75389-310.1007/978-3-642-75389-3_5

Lewis, S. L., Edwards, D. P., and Galbraith, D. (2015). Increasing human dominance of tropical forests. *Science* 349, 827–832. doi:10.1126/science.aaa9932

Lewis, S. L., Lopez-Gonzalez, G., Sonké, B., Affum-Baffoe, K., Baker, T. R., Ojo, L. O., et al. (2009). Increasing carbon storage in intact African tropical forests. *Nature* 457, 1003–1006. doi:10.1038/nature07771

Livengood, T. A., Deming, L. D., A'Hearn, M. F., Charbonneau, D., Hewagama, T., Lisse, C. M., et al. (2011). Properties of an Earth-Like Planet Orbiting a Sun-Like Star: Earth Observed by the EPOXI Mission. *Astrobiology* 11, 907–930. doi:10.1089/ast.2011.0614

Marshak, A., Herman, J., Adam, S., Karin, B., Carn, S., Cede, A., et al. (2018). Earth Observations from DSCOVR EPIC Instrument. *BAMS* 99, 1829–1850. doi:10.1175/BAMS-D-17-0223.1

Marshak, A., Krotkov, N., Gorkavyi, N., Marchenko, S., Vasilkov, A., Knyazikhin, Y., et al. (2020). "Whole Earth imaging from the Moon South Pole (EPIC-Moon)," in *Whitepaper*. https://www.lpi.usra.edu/announcements/artemis/whitepapers/2054.pdf.

Marshak, A., Várnai, T., and Kostinski, A. (2017). Terrestrial glint seen from deep space: oriented ice crystals detected from the Lagrangian point. *Geophys. Res. Lett.* 44, 5197–5202. doi:10.1002/2017GL073248

Morton, D. C., Nagol, J., Carabajal, C. C., Rosette, J., Rosette, J., Palace, M., et al. (2016). Morton et al. reply. *Nature* 531, E6. doi:10.1038/nature16458

Myneni, R. B., Marshak, A. L., and Knyazikhin, Y. V. (1991). Transport theory for a leaf canopy of finite-dimensional scattering centers. *J. Quantitative Spectrosc. Radiative Transfer* 46, 259–280. doi:10.1016/0022-4073(91)90091-4

Myneni, R. B., Yang, W., Nemani, R. R., Huete, A. R., Dickinson, R. E., Knyazikhin, Y., et al. (2007). Large seasonal swings in leaf area of Amazon rainforests. *Proc. Natl. Acad. Sci.* 104, 4820–4823. doi:10.1073/pnas.0611338104

National Academies of Sciences (2018). *Thriving on Our Changing Planet: A Decadal Strategy for Earth Observation from Space*. Washington, DC: The National Academies Press. doi:10.17226/24938

Pan, Y., Birdsey, R. A., Fang, J., Houghton, R., Kauppi, P. E., Kurz, W. A., et al. (2011). A Large and Persistent Carbon Sink in the World's Forests. *Science* 333, 988–993. doi:10.1126/science.1201609

Pavolonis, M. J., Sieglaff, J., and Cintineo, J. (2018). Automated Detection of Explosive Volcanic Eruptions Using Satellite-Derived Cloud Vertical Growth Rates. *Earth Space Sci.* 5, 903–928. doi:10.1029/2018EA000410

Pisek, J., Arndt, S. K., Erb, A., Pendall, E., Schaaf, C., Wardlaw, T. J., et al. (2021). Exploring the Potential of DSCOVR EPIC Data to Retrieve Clumping Index in Australian Terrestrial Ecosystem Research Network Observing Sites. *Front. Remote Sens.* 2, 652436. doi:10.3389/frsen.2021.652436

Qin, W., Gerstl, S. A. W., Deering, D. W., and Goel, N. S. (2002). Characterizing leaf geometry for grass and crop canopies from hotspot observations: A simulation study. *Remote Sensing Environ.* 80, 100–113. doi:10.1016/S0034-4257(01)00291-7

Qin, W., Goel, N. S., and Wang, B. (1996a). The hotspot effect in heterogeneous vegetation canopies and performances of various hotspot models. *Remote Sensing Rev.* 14, 283–332. doi:10.1080/02757259609532323

Qin, W. H., Goel, N. S., and Wang, B. Q. (1996b). Estimation of leaf size from hotspot observations. *Remote Sensing a Sust. Future* Vols I - Iv, 1645–1647. Igarss '96 - 1996 International Geoscience and Remote Sensing Symposium.

Richard, D. T., Glenar, D. A., Stubbs, T. J., Davis, S. S., and Colaprete, A. (2011). Light scattering by complex particles in the Moon's exosphere: Toward a taxonomy of models for the realistic simulation of the scattering behavior of lunar dust. *Planet. Space Sci.* 59, 1804–1814. doi:10.1016/j.pss.2011.01.003

Robinson, T. D., Meadows, V. S., and Crisp, D. (2010). Detecting Oceans on Extrasolar Planets Using the Glint Effect. *ApJ*, 721, L67–L71. doi:10.1088/2041-8205/721/1/L67

Ross, J. K., and Marshak, A. L. (1988). Calculation of canopy bidirectional reflectance using the Monte Carlo method. *Remote Sensing Environ.* 24, 213–225. doi:10.1016/0034-4257(88)90026-0

Ross, J., and Marshak, A. (1991). Influence of the Crop Architecture Parameters on Crop Brdf - a Monte-Carlo Simulation. *Phys. Measurements Signatures Remote Sensing* 1 and 2, 357–360.

Sagan, C., Thompson, W. R., Carlson, R., Gurnett, D., and Hord, C. (1993). A search for life on Earth from the Galileo spacecraft. *Nature* 365, 715–721. doi:10.1038/365715a0

Saleska, S. R., Wu, J., Guan, K., Araujo, A. C., Huete, A., Nobre, A. D., et al. (2016). Dry-season greening of Amazon forests. *Nature* 531, E4–E5. doi:10.1038/nature16457

Samanta, A., Knyazikhin, Y., Xu, L., Dickinson, R. E., Fu, R., Costa, M. H., et al. (2012). Seasonal changes in leaf area of Amazon forests from leaf flushing and abscission. *J. Geophys. Res.* 117, G01015. doi:10.1029/2011JG001818

Schull, M. A., Knyazikhin, Y., Xu, L., Samanta, A., Carmona, P. L., Lepine, L., et al. (2011). Canopy spectral invariants, Part 2: Application to classification of forest types from hyperspectral data. *J. Quantitative Spectrosc. Radiative Transfer* 112, 736–750. doi:10.1016/j.jqsrt.2010.06.004

Song, W., Knyazikhin, Y., Wen, G., Marshak, A., Mõttus, M., Yan, K., et al. (2018). Implications of Whole-Disc DSCOVR EPIC Spectral Observations for Estimating Earth's Spectral Reflectivity Based on Low-Earth-Orbiting and Geostationary Observations. *Remote Sensing* 10, 1594. doi:10.3390/rs10101594

Speyerer, E. J., Povilaitis, R. Z., Robinson, M. S., Thomas, P. C., and Wagner, R. V. (2016). Quantifying crater production and regolith overturn on the Moon with temporal imaging. *Nature* 538, 215–218. doi:10.1038/nature19829

Torres, O., Bhartia, P. K., Taha, G., Jethva, H., Das, S., Colarco, P., et al. (2020). Stratospheric Injection of Massive Smoke Plume from Canadian Boreal Fires in 2017 as Seen by DSCOVR-EPIC, CALIOP, and OMPS-LP Observations. *J. Geophys. Res. Atmos.* 125, 2020jd032579. doi:10.1029/2020JD032579

Tsuda, T. T., Hozumi, Y., Kawaura, K., Hosokawa, K., Suzuki, H., and Nakamura, T. (2018). Initial report on polar mesospheric cloud observations by Himawari-8. *Atmos. Meas. Tech.* 11, 6163–6168. doi:10.5194/amt-11-6163-2018

Varnai, T., Kostinski, A. B., and Marshak, A. (2020). Deep space observations of sun glints from marine ice clouds. *IEEE Geosci. Remote Sensing Lett.* 17 (5), 735–739. doi:10.1109/LGRS.2019.2930866

Walker, J. (2021). *Earth and Moon Viewer*. https://www.fourmilab.ch/cgi-bin/Earth.

Williams, D. M., and Gaidos, E. (2008). Detecting the glint of starlight on the oceans of distant planets. *Icarus* 195, 927–937. doi:10.1016/j.icarus.2008.01.002

Yang, B., Knyazikhin, Y., Mõttus, M., Rautiainen, M., Stenberg, P., Yan, L., et al. (2017). Estimation of leaf area index and its sunlit portion from DSCOVR EPIC data: Theoretical basis. *Remote Sensing Environ.* 198, 69–84. doi:10.1016/j.rse.2017.05.033